Research Paper
Computational Methods for Differential Equations
http://cmde.tabrizu.ac.ir
Vol. *, No. *, *, pp. 1-16
DOI:10.22034/cmde.2026.62667.2775

Numerical investigation of thermal behavior in hyperthermia treatment

Swarn Singh[1,*], Suruchi Singh[2], and Asha Kumari[3]

[1]Department of Mathematics, Sri Venkateswara College, University of Delhi, Delhi 110021, India.

[2]Department of Mathematics, Aditi Mahavidyalaya, University of Delhi, Delhi 110039, India.

[3]Department of Mathematics, Faculty of Mathematical Sciences, University of Delhi, Delhi 110007, India.

Abstract

Cancer is a life-threatening disease, and hyperthermia is one of the therapeutic procedures used in cancer treatment. Understanding and accurately predicting the temperature distribution in biological tissues during hyperthermia treatment is therefore important. Heat transfer in biological tissue is mathematically modelled using Pennes' bioheat transfer equation (PBHTE). In this paper, we present a high-order numerical method for solving the PBHTE with discontinuous thermal properties. Problems with known analytical solutions are considered to verify the accuracy and convergence order of the proposed method.
The method is subsequently applied to investigate the temperature distribution in a biological tissue consisting of two regions. The first region represents diseased tissue in which heat is generated during hyperthermia treatment, while the second represents healthy tissue. The temperature behaviour is examined for both constant and variable heat generation produced by an external heat source. The influence of blood perfusion on the resulting temperature distribution is also investigated.

Keywords. Hyperthermia, Pennes' bioheat transfer equation, Interface, Crank–Nicolson method, Finite difference method, Maximum absolute error, Temperature, Fourth-order method.

2010 Mathematics Subject Classification. 65M06, 65M12, 35K20.

1. Introduction

Partial differential equations act as a building block for modeling physical phenomena and have vast applications in the real world. The basic world problems can be categorized into various physical problems, biological problems, geographical problems, mathematical problems, etc. The exchange of energy is explained by the law of thermodynamics, which says that energy can be exchanged between physical systems as heat and work. The law of conservation of energy explains that energy can neither be created nor destroyed; it can only be transferred from a region of higher potential to a region of lower potential. However, this rate of transfer depends on a lot of factors, like the thermal property of the material through which the heat is flowing, the boundary conditions, and inter-molecular interaction. The mode of heat transfer could be conduction, convection, or radiation, depending on the molecular interaction.

As all the partial differential equations do not guarantee to have an analytical solution. So the best thing to do is to try to find a numerical solution that is more accurate to the analytical solution. Due to the advancement of science, there is vast development of numerical methods in the field of computational mathematics.

Heat transfer in living tissues is a vital topic in mathematical modeling with great practical importance in bio-engineering. Pennes [12] introduced the parabolic heat transfer equation in biological tissue.

In the paper [16], to test the effects of variations in thermal physical properties on skin temperature and burn predictions, multiple-layer, variable property finite element model of the heat transfer was discussed. Many authors [10, 13, 15], discussed thermal wave model of bioheat transfer to investigate the wave like behaviors of heat transfer

Received: 26 July 2024; Accepted: 09 August 2026.
∗ Corresponding author. Email: ssingh@svc.ac.in.

occurred in thermal injury of biological bodies. To predict rise in temperature in biological tissues during hyperthermia treatment, dual-phase-lag model is studied using a hybrid numerical scheme based on the Laplace transform [9]. Pennes bioheat equation (PBHTE) equation was used to study several typical bioheat transfer processes, which are often encountered in cancer hyperthermia, laser surgery, thermal comfort analysis, and tissue thermal parameter estimation [3]. Authors in the paper [18], predicted the temperature response of the biological tissues by using the space-dependent blood perfusion term in Pennes bioheat equation theoretically.

In isotropic mediums with effective thermal properties, solutions of the Pennes bioheat equation are derived using Green's function in the paper [4]. Hyperthermia also plays an important role in fibromyalgia and ankylosing spondylitis therapy [5]. In hyperthermia the target tissue is heated in the range of $41^0C - 45^0C$ [17] approximately. Although the excess heat is applied for therapeutic purposes, any temperature above the body temperature is considered excessive and may cause damage to healthy tissue as well. So, it is necessary to study the pattern of temperature in the tissue. The authors in the paper [14] derived the exact solution of the one-dimensional Pennes bioheat transfer equation for single-layered biological tissue with the periodic heat flux boundary heating condition on the skin surface. Mohanty et.al. [11], developed high-order compact difference scheme for a parabolic partial differential equation. In order to solve partial differential equations with discontinuous coefficients and singular sources, an immersed interface method was developed in [7, 8].

In this paper, we present a high-order compact finite difference method for the bioheat transfer equation in multi-layered tissue. We investigate the temperature distribution numerically in the biological tissue. In section 2 of this paper, we explain the bioheat transfer model that will be our main equation to study the behavior of temperature in biological tissue. In section 3, we formulate a numerical method in the absence of irregularities. Stability analysis of the method is done in section 4. In section 5, we extend the numerical formulation to the irregular case. After that, in section 6 we solve some numerical examples to show the efficacy of the method. In section 7, we explain the application of the method on the bioheat equation by considering a cancerous tissue embedded in a healthy tissue. At last, in section 8, we write conclusion of this paper.

2. Bioheat Transfer Model

The Pennes bioheat transfer model [12] is given by the equation

$$\rho C \frac{\partial T}{\partial t} = \nabla \cdot (\kappa \nabla T) + q_{met} + q_{per} + P, \tag{2.1}$$

where,

- T**::** represents temperature (℃),
- ρ**,** C**,** κ **::** represents the density (kg/m^3), the specific heat $(J/(kg.K))$, and the tissue thermal conductivity $W/(mK)$, respectively,
- $\nabla \cdot (\kappa \nabla T)$**::** gives the theal conduction inside the tissue after all the local spots of heat generation are identified,
- $\frac{\partial T}{\partial t}$**::** represents the rate of change of temperature with respect to time,
- P**::** represents heat generation due to external heat source (W/m^3),
- q_{met}**::** the heat generation rate, heat generated due to metabolic activity happening in the tissue,
- q_{per}**::** is the heat transfer rate per unit volume of tissue due to blood perfusion,

and

$$q_{per} = -\rho_b C_b \omega_b (T - T_b).$$

Here, $(T - T_b)$ is the difference between local tissue temperature and that of arterial blood. ρ_b is the mass flow rate of blood per unit volume of tissue and C_b is the blood-specific heat, ω_b is the blood perfusion rate. In our problem, we will ignore heat generation due to metabolic activity. i.e $q_{met} = 0$.

So, the Eq. (2.1) in one dimension becomes

$$\rho C \frac{\partial T}{\partial t} = \nabla \cdot (\kappa \nabla T) - \rho_b C_b \omega_b (T - T_b) + P, x \in \Omega, t > 0. \tag{2.2}$$

The boundary conditions are given by

$$T(x,0) = T_0,\ for\ x \in \Omega, \tag{2.3}$$

where T_0 is the normal body temperature.

Taking $\Omega = [a,b]$, at the boundary $x = a$, the temperature is finite $T(a,t) < \infty$, for $t > 0$, and at the boundary $x = b$, $T(b,t) = T_0$, for $t > 0$.

3. Numerical Formulation Away from the Interface

In the case, where there is no irregularity and the solution of the differential equation (2.2) belongs to $C^6(\Omega)$. We re-write the differential equation (2.2) as

$$\beta T_t = \nabla(\kappa \nabla T) - \gamma T - f(x,t), \quad x \in \Omega, \quad t > 0, \tag{3.1}$$

where $\beta = \rho C$, $\gamma = \rho_b C_b \omega_b$, $f(x,t) = \rho_b C_b \omega_b T_b + P$, with appropriate initial and boundary conditions. Here, κ is assumed to be linear function of x, therefore the Eq. (3.1) can further be re-written as

$$\begin{aligned} \kappa T_{xx} + \kappa' T_x &= \beta T_t + \gamma T + f(x,t) \\ &\equiv g(x,t,T,T_t), \qquad x \in \Omega,\ t > 0. \end{aligned} \tag{3.2}$$

The domain $\Omega = [a,b]$ has been divided into N sub-intervals $[x_{l-1}, x_l]$ of equal length, where $x_l = a + lh, l = 1,2,\ldots,N$. $h = \frac{b-a}{N}$ is the length of the sub-intervals. Let us assume Δt to be the time step size and $t_j = j\Delta t$ are the time levels, j is a non-negative integer. The value of the functions T and f at the grid point (x_l, t_j) are denoted by T_l^j and f_l^j, respectively.

The following compact scheme gives fourth-order approximations to the second-order derivative T_{xx} at grid point (x_l, t_j):

$$\frac{1}{h^2}\left(1 + \frac{\delta_x^2}{12}\right)^{-1} \delta_x^2 T_l^j = T_{xx_l}^j, \tag{3.3}$$

where,

$$\delta_x T_l^j = T_{l+\frac{1}{2}}^j - T_{l-\frac{1}{2}}^j.$$

We also use the following approximations for the first derivative T_x:

$$T_{x_{l\pm1}}^j = \frac{1}{2h}(2\mu_x\delta_x \pm 2\delta_x^2)T_l^j, \tag{3.4}$$

and

$$T_{x_l}^j = \frac{T_{l+1}^j - T_{l-1}^j}{2h} - \frac{h}{20\kappa_l}(\kappa_{l+1}T_{xx_{l+1}}^j - \kappa_{l-1}T_{xx_{l-1}}^j) + \frac{\kappa'}{10\kappa_l}\delta_x^2 T_l^j, \tag{3.5}$$

where $\mu_x T_l^j = \frac{T_{l+\frac{1}{2}}^j + T_{l-\frac{1}{2}}^j}{2}$.

So, using the approximations from the Eqs. (3.3), (3.4), and (3.5), we obtain the following discretization of the differential equation (3.1),

$$\begin{aligned} \left(\frac{12\kappa_l}{h^2} - \frac{2\kappa'^2}{\kappa_l} - \gamma\right)\delta_x^2 T_l^j = \left(12 + \delta_x^2 - \frac{h\kappa'}{2\kappa_l}(2\mu_x\delta_x)\right)\beta T_{t\ l}^j + 12\gamma T_l^j - \frac{\kappa'}{2h\kappa_l}\left(12\kappa_l - \gamma h^2\right)(2\mu_x\delta_x)T_l^j \\ + \left(\left(1 + \frac{h\kappa'}{2\kappa_l}\right)f_{l-1}^j + 10 f_l^j + \left(1 - \frac{h\kappa'}{2\kappa_l}\right)f_{l+1}^j\right), \end{aligned} \tag{3.6}$$

for $l = 1,2,\ldots,N, j = 1,2,3,\ldots$.

Next, applying the Crank-Nicolson method in time direction on the Eq. (3.6), we obtain the following discretization to the partial differential equation (3.1), at the grid point (x_l, t_j),

$$\begin{aligned}\left(\frac{12\kappa_l}{h^2} - \frac{2\kappa'^2}{\kappa_l} - \frac{\gamma}{12}\right)\frac{\delta_x^2 T_l^j + \delta_x^2 T_l^{j+1}}{2} &= \beta\left(12 + \delta_x^2 - \frac{h\kappa'}{2\kappa_l}(2\mu_x\delta_x)\right)\frac{T_l^{j+1} - T_l^j}{\Delta t} + 12\gamma\frac{T_l^j + T_l^{j+1}}{2} \\ &- \frac{\kappa'}{4h\kappa_l}\left(12\kappa_l - \gamma h^2\right)\left(2\mu_x\delta_x T_l^j + 2\mu_x\delta_x T_l^{j+1}\right) \\ &+ \left(\left(1 + \frac{h\kappa'}{2\kappa_l}\right)\frac{f_{l-1}^j + f_{l-1}^{j+1}}{2} + 10\frac{f_l^j + f_l^{j+1}}{2} + \left(1 - \frac{h\kappa'}{2\kappa_l}\right)\frac{f_{l+1}^j + f_{l+1}^{j+1}}{2}\right), \quad (3.7)\end{aligned}$$

for $l = 1, 2, \ldots, N, j = 0, 1, 2, \ldots$.

The Eq. (3.7) can further be re-written as

$$\begin{aligned}&\left(\frac{12\kappa_l}{h^2} - \frac{2\kappa'^2}{\kappa_l} - \gamma\right)\left\{\frac{T_{l-1}^{j+1} - 2T_l^{j+1} + T_{l+1}^{j+1}}{2} + \frac{T_{l-1}^j - 2T_l^j + T_{l+1}^j}{2}\right\} \\ &= \beta\left((1 + \frac{h\kappa'}{2\kappa_l})\frac{T_{l-1}^{j+1} - T_{l-1}^j}{\Delta t} + 10\frac{T_l^{j+1} - T_l^j}{\Delta t} + (1 - \frac{h\kappa'}{2\kappa_l})\frac{T_{l+1}^{j+1} - T_{l+1}^j}{\Delta t}\right) \\ &+ 12\gamma\frac{T_l^j + T_l^{j+1}}{2} - \frac{\kappa'}{2h\kappa_l}\left(12\kappa_l - \gamma h^2\right)\left(\frac{T_{l+1}^j + T_{l+1}^{j+1}}{2} - \frac{T_{l-1}^j + T_{l-1}^{j+1}}{2}\right) \\ &+ \left(\left(1 + \frac{h\kappa'}{2\kappa_l}\right)\frac{f_{l-1}^j + f_{l-1}^{j+1}}{2} + 10\frac{f_l^j + f_l^{j+1}}{2} + \left(1 - \frac{h\kappa'}{2\kappa_l}\right)\frac{f_{l+1}^j + f_{l+1}^{j+1}}{2}\right). \quad (3.8)\end{aligned}$$

The method given by the Eq. (3.8) is of order four for $k \propto h^2$, according to the Taylor's theorem. Unconditionally stability of the difference method (3.8) can be confirmed easily, using Von Neumann stability analysis.

At all time levels, we obtain a tri-diagonal structure of the coefficient matrices that can be solved using the given initial and boundary conditions.

4. Stability analysis

In this section, we use Von-Neumann stability analysis to examine the stability of our method and try to get deeper insight into its behavior. Let us consider the homogeneous part of the differential equation. The method given by the Eq. (3.8), becomes

$$\begin{aligned}&\left(\frac{12\kappa_l}{h^2} - \frac{2\kappa'^2}{\kappa_l} - \gamma\right)\left(\frac{T_{l-1}^{j+1} - 2T_l^{j+1} + T_{l+1}^{j+1}}{2} + \frac{T_{l-1}^j - 2T_l^j + T_{l+1}^j}{2}\right) \\ &= \beta\left((1 + \frac{h\kappa'}{2\kappa_l})\frac{T_{l-1}^{j+1} - T_{l-1}^j}{\Delta t} + 10\frac{T_l^{j+1} - T_l^j}{\Delta t} + (1 - \frac{h\kappa'}{2\kappa_l})\frac{T_{l+1}^{j+1} - T_{l+1}^j}{\Delta t}\right) \\ &+ 12\gamma\frac{T_l^j + T_l^{j+1}}{2} - \frac{\kappa'}{2h\kappa_l}\left(12\kappa_l - \gamma h^2\right)\left(\frac{T_{l+1}^j + T_{l+1}^{j+1}}{2} - \frac{T_{l-1}^j + T_{l-1}^{j+1}}{2}\right). \quad (4.1)\end{aligned}$$

After re-arranging the terms of the Eq. (4.1),

$$\begin{aligned}&\left(\frac{A}{2} - \frac{\beta(1+\delta)}{\Delta t} - \frac{B}{2}\right)T_{l-1}^{j+1} - \left(A + \frac{10\beta}{\Delta t} + 6\gamma\right)T_l^{j+1} + \left(\frac{A}{2} - \frac{\beta(1-\delta)}{\Delta t} + \frac{B}{2}\right)T_{l+1}^{j+1} \\ &= -\left(\frac{A}{2} + \frac{\beta(1+\delta)}{\Delta t} - \frac{B}{2}\right)T_{l-1}^j + \left(A - \frac{10\beta}{\Delta t} + 6\gamma\right)T_l^j - \left(\frac{A}{2} + \frac{\beta(1-\delta)}{\Delta t} + \frac{B}{2}\right)T_{l+1}^j. \quad (4.2)\end{aligned}$$

$$A = \frac{12\kappa_l}{h^2} - \frac{2(\kappa')^2}{\kappa_l} - \gamma, \tag{4.3}$$

$$\delta = \frac{h\kappa'}{2\kappa_l}, \tag{4.4}$$

$$B = \frac{\kappa'}{2h\kappa_l}\left(12\kappa_l - \gamma h^2\right). \tag{4.5}$$

Let us consider the trial solution to be,

$$T_l^j = \xi^j e^{iklh}. \tag{4.6}$$

where $i = \sqrt{-1}$, ξ is the amplification factor, and k is wave number, and h is the spatial distance. After substituting the value of the trial solution for T_l^j in the Eq. (4.2) we get,

$$\begin{aligned}
&\left(\frac{A}{2} - \frac{\beta(1+\delta)}{\Delta t} - \frac{B}{2}\right)\xi^{j+1}e^{ik(l-1)h} - (A + \frac{10\beta}{\Delta t} + 6\gamma)\xi^{j+1}e^{iklh} + \left(\frac{A}{2} - \frac{\beta(1-\delta)}{\Delta t} + \frac{B}{2}\right)\xi^{j+1}e^{ik(l+1)h} \\
&= \left(-\frac{A}{2} - \frac{\beta(1+\delta)}{\Delta t} + \frac{B}{2}\right)\xi^{j}e^{ik(l-1)h} + \left(A - \frac{10\beta}{\Delta t} + 6\gamma\right)\xi^{j}e^{iklh} - \left(\frac{A}{2} + \frac{\beta(1-\delta)}{\Delta t} + \frac{B}{2}\right)\xi^{j}e^{ik(l+1)h}.
\end{aligned} \tag{4.7}$$

After simplification the amplification factor becomes,

$$\xi = \frac{\left(A - \frac{10\beta}{\Delta t} + 6\gamma\right) + \left(-A - 2\frac{\beta(1+\delta)}{\Delta t}\right)\cos(kh) + i\left(-B + 2\frac{\beta\delta}{\Delta t}\right)\sin(kh)}{\left(-A - \frac{10\beta}{\Delta t} - 6\gamma\right) + \left(A - 2\frac{\beta(1-\delta)}{\Delta t}\right)\cos(kh) + iB\sin(kh)}. \tag{4.8}$$

Therefore, we obtain

$$\begin{aligned}
|\xi|^2 &= \frac{\left[\left(A - \frac{10\beta}{\Delta t} + 6\gamma\right) + \left(-A - 2\frac{\beta(1+\delta)}{\Delta t}\right)\cos(kh)\right]^2 + \left[\left(-B + 2\frac{\beta\delta}{\Delta t}\right)\sin(kh)\right]^2}{\left[\left(-A - \frac{10\beta}{\Delta t} - 6\gamma\right) + \left(A - 2\frac{\beta(1-\delta)}{\Delta t}\right)\cos(kh)\right]^2 + \left[B\sin(kh)\right]^2} \\
&= \frac{\left[A(1-\cos(kh)) - \frac{\beta}{\Delta t}(10 + 2\cos(kh)) + 6\gamma\right]^2 + \left[\left(\frac{2\beta\delta}{\Delta t} - B\right)\sin(kh)\right]^2}{\left[A(1-\cos(kh)) + \frac{\beta}{\Delta t}(10 + 2\cos(kh)) + 6\gamma\right]^2 + \left[\left(\frac{2\beta\delta}{\Delta t} + B\right)\sin(kh)\right]^2}.
\end{aligned} \tag{4.9}$$

Let

$$N = \left[A(1-\cos(kh)) - \frac{\beta}{\Delta t}(10 + 2\cos(kh)) + 6\gamma\right]^2 + \left[\left(\frac{2\beta\delta}{\Delta t} - B\right)\sin(kh)\right]^2,$$

and

$$D = \left[A(1-\cos(kh)) + \frac{\beta}{\Delta t}(10 + 2\cos(kh)) + 6\gamma\right]^2 + \left[\left(\frac{2\beta\delta}{\Delta t} + B\right)\sin(kh)\right]^2.$$

Then,

$$D - N = \frac{4\beta}{\Delta t}\left[(10 + 2\cos(kh))\left\{A(1-\cos(kh)) + 6\gamma\right\} + 2\delta B\sin^2(kh)\right].$$

Since $10 + 2\cos(kh) > 0$, $1 - \cos(kh) \geq 0$, $\sin^2(kh) \geq 0$, $\kappa > 0$, we can clearly see that, as $h \to 0$,

$$|\xi| \leq 1. \tag{4.10}$$

Hence, we observe that our method is unconditionally stable.

5. Extension of the numerical formulation to the irregular case

Now, we consider the case, when the coefficients get affected due to the presence of an interface between two different materials. The interface act as the point of discontinuity for the coefficients of the Eq. (3.1). The interface disconnect the region at point α and separate them into two parts $\Omega^- = [a, \alpha)$ and $\Omega^+ = (\alpha, b]$ at time t. Using the concept of the conservation law, the temperature must be continuous. To maintain that continuity of temperature in the whole domain, we must have $[T] = 0$, as T represents a physical quantity. Here, $[T]$ represents the jump in $T(x)$ at α:

$$[T] = T^+ - T^-, \tag{5.1}$$

where T^+ denotes the right hand limit of the temperature when x approaches to α and T^- denotes left hand limit of the temperature when x approaches to α.

In addition to this, continuity of heat flux is also applied on the interior of the tissue. So,

$$[\kappa \nabla T] = 0. \tag{5.2}$$

Let us assume that the α is situated between grid points $x_{\bar{l}}$ and $x_{\bar{l}+1}$, respectively, as the interface may not be appropriately laying on any of the grid points, as shown in Figure 1. Using Taylor's expansion about $x = \alpha$ and

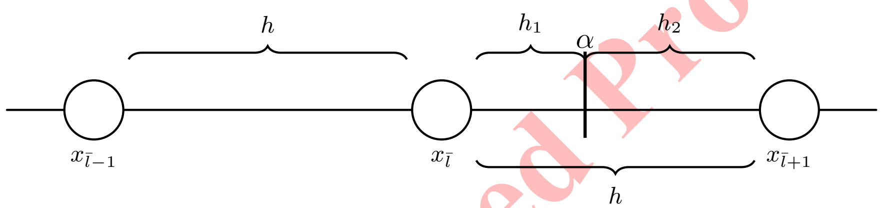

Figure 1. Interface α lying between nodes $x_{\bar{l}}$ and $x_{\bar{l}+1}$.

neglecting fourth-order terms, we have

$$T_{\bar{l}} = T^- - T_x^- h_1 + \frac{1}{2} T_{xx}^- h_1^2 - \frac{1}{6} T_{xxx}^- h_1^3, \tag{5.3}$$

$$T_{\bar{l}+1} = T^+ + T_x^+ h_2 + \frac{1}{2} T_{xx}^+ h_2^2 + \frac{1}{6} T_{xxx}^+ h_2^3, \tag{5.4}$$

$$T_{\bar{l}-1} = T^- - T_x^- h_3 + \frac{1}{2} T_{xx}^- h_3^2 - \frac{1}{6} T_{xxx}^- h_3^3. \tag{5.5}$$

where $h_1 = \alpha - x_{\bar{l}}$ $h_2 = x_{\bar{l}+1} - \alpha$ and $h_3 = h + h_2$.

Using Taylor's expansions for T_t about $x = \alpha$, we have

$$T_{t_{\bar{l}}} = T_t^- - T_{tx}^- h_1 + \frac{1}{2} T_{txx}^- h_1^2 - \frac{1}{6} T_{txxx}^- h_1^3, \tag{5.6}$$

$$T_{t_{\bar{l}+1}} = T_t^+ + T_{tx}^+ h_2 + \frac{1}{2} T_{txx}^+ h_2^2 + \frac{1}{6} T_{txxx}^+ h_2^3, \tag{5.7}$$

$$T_{t\bar{l}-1} = T_t{}^- - T_{tx}^- h_3 + \frac{1}{2} T_t xx^- h_3^2 - \frac{1}{6} T_{txxx}^- h_3^3. \tag{5.8}$$

As our problem is continuous in time from Eqs. (5.1) and (5.2), we have $T_t^+ = T_t^-$ and $(\kappa T_{tx})^+ = (\kappa T_{tx})^-$.

The presence of interface is affecting the method when we are considering the two sets of grid points $x_{\bar{l}-1}$, $x_{\bar{l}}$ and $x_{\bar{l}+1}$, and $x_{\bar{l}}$, $x_{\bar{l}+1}$ and $x_{\bar{l}+2}$.

From the Eqs. (5.3)-(5.5) and the differential Eq. (3.2), we can write

$$T_{\bar{l}+1} = T^- + X_1 T_x^- + Y_1, \tag{5.9}$$
$$T_{\bar{l}} = T^- + X_2 T_x^- + Y_2, \tag{5.10}$$
$$T_{\bar{l}-1} = T^- + X_3 T_x^- + Y_3, \tag{5.11}$$

where,

$$X_1 = h_2 - \frac{h_2^2 \kappa^{+'}}{2\kappa^+} + \frac{2h_2^3 \kappa^{+'2}}{3!\kappa^{+2}}, \qquad Y_1 = \left(\frac{h_2^2}{2\kappa^+} - \frac{2h_2^3\kappa^{+'}}{3!\kappa^{+2}}\right) g^+ + \frac{h_2^3}{3!\kappa^+} g_x^+, \tag{5.12}$$
$$X_2 = -\left(h_1 + \frac{h_1^2 \kappa^{-'}}{2\kappa^-} + \frac{2h_1^3 \kappa^{-'2}}{3!\kappa^{-2}}\right), \qquad Y_2 = \left(\frac{h_1^2}{2\kappa^-} + \frac{2h_1^3\kappa^{-'}}{3!\kappa^{-2}}\right) g^- - \frac{h_1^3}{3!\kappa^-} g_x^-, \tag{5.13}$$
$$X_3 = -\left(h_3 + \frac{h_3^2 \kappa^{-'}}{2\kappa^-} + \frac{2h_3^3 \kappa^{-'2}}{3!\kappa^{-2}}\right), \qquad Y_3 = \left(\frac{h_3^2}{2\kappa^-} + \frac{2h_3^3\kappa^{-'}}{3!\kappa^{-2}}\right) g^- - \frac{h_3^3}{3!\kappa^-} g_x^-. \tag{5.14}$$

The following relations can be obtained using the jump conditions and the Taylors' expansions:

$$T^- = \frac{h_1 T_{l-1} - h_3 T_l}{h_1 - h_3}, \tag{5.15}$$
$$T^+ = \frac{\kappa^+ h_1 T_{l+1} + \kappa^- h_2 T_l}{\kappa^+ h_1 + \kappa^- h_2}, \tag{5.16}$$
$$T^+ = \frac{\kappa^+ h_3 T_{l+1} + \kappa^- h_2 T_{l-1}}{\kappa^+ h_3 + \kappa^- h_2}. \tag{5.17}$$

Also, using Taylors's expansions we can get the following approximations:

$$g_x^- = \frac{g^- - g_{l-1}}{h_3} + O(h^2), \tag{5.18}$$
$$g_x^- = \frac{g^- - g_l}{h_1} + O(h^2), \tag{5.19}$$
$$g_x^+ = \frac{g_{l+1} - g^+}{h_2} + O(h^2). \tag{5.20}$$

Using Eqs. (5.15)-(5.20), we can write Y_1 , Y_2 and Y_3 from Equations (5.12)-(5.14), as:

$$\begin{aligned} Y_1 &= \frac{h_2^2}{3!\kappa^+}\left[\left(3 - \frac{2h_2\kappa^{+'}}{\kappa^+}\right) g^+ + h_2 \frac{g_{l+1} - g^+}{h_2}\right] \\ &= \frac{h_2^2}{3!\kappa^+}\left[\left(2 - \frac{2h_2\kappa^{+'}}{\kappa^+}\right)\left(\beta^+ \frac{\kappa^+ h_1 T_{tl+1} + \kappa^- h_2 T_{tl}}{\kappa^+ h_1 + \kappa^- h_2} \quad + \gamma^+ \frac{\kappa^+ h_1 T_{l+1} + \kappa^- h_2 T_l}{\kappa^+ h_1 + \kappa^- h_2} + f^+\right) + g_{l+1}\right], \\ Y_2 &= \frac{h_1^2}{3!\kappa^-}\left[\left(3 + \frac{2h_1\kappa^{-'}}{\kappa^-}\right) g^- - h_1 \frac{g^- - g_l}{h_1}\right] \\ &= \frac{h_1^2}{3!\kappa^-}\left[\left(2 + \frac{2h_1\kappa^{-'}}{\kappa^-}\right)(\beta^- \frac{h_1 T_{tl-1} - h_3 T_{tl}}{h_1 - h_3} + \gamma^- \frac{h_1 T_{l-1} - h_3 T_l}{h_1 - h_3} + f^-) + g_l\right], \end{aligned} \tag{5.21}$$

and

$$
\begin{aligned}
Y_3 &= \frac{h_3^2}{3!\kappa^-}\left[\left(3+\frac{2h_3\kappa^{-'}}{\kappa^-}\right)g^- - h_3\frac{g^- - g_{l-1}}{h_3}\right]\\
&= \frac{h_3^2}{3!\kappa^-}\left[\left(2+\frac{2h_3\kappa^{-'}}{\kappa^-}\right)g^- + g_{l-1}\right]\\
&= \frac{h_3^2}{3!\kappa^-}\left[\left(2+\frac{2h_3\kappa^{-'}}{\kappa^-}\right)\left(\beta^-\left(\frac{h_1T_{tl-1}-h_3T_{tl}}{h}\right)\ +\gamma^-\left(\frac{h_1T_{l-1}-h_3T_l}{h}\right)+f^-\right)+g_{l-1}\right]\\
&= \frac{h_3^2}{3!\kappa^-}\left[\left[1-\frac{h_1}{h}\left(2+\frac{2h_3\kappa^{-'}}{\kappa^-}\right)\right]\left(\beta^-T_{tl-1}+\gamma^-T_{l-1}\right)\ +\frac{h_3}{h}\left(2+\frac{2h_3\kappa^{-'}}{\kappa^-}\right)\left(\beta^-T_{tl}+\gamma^-T_l\right)\right]\\
&+\frac{h_3^2}{3!\kappa^-}\left[\left(2+\frac{2h_3\kappa^{-'}}{\kappa^-}\right)f^- + f_{l-1}\right]
\end{aligned}
$$

Subtracting Eq. (5.9) from Eq. (5.10), we obtain

$$
T_{\bar{l}+1}-T_{\bar{l}} = (X_1-X_2)T_x^- + Y_1 - Y_2 \tag{5.22}
$$

Subtracting Eq. (5.10) and from the Eq. (5.11), we get

$$
T_{\bar{l}-1}-T_{\bar{l}} = (X_3-X_2)T_x + Y_3 - Y_2 \tag{5.23}
$$

Now, we eliminate T_x^- from the Eqs. (5.22) and (5.23) and get

$$
(X_2-X_1)T_{\bar{l}-1}+(X_1-X_3)T_{\bar{l}}+(X_3-X_2)T_{\bar{l}+1} = (Y_1-Y_2)(X_3-X_2)-(Y_3-Y_2)(X_1-X_2). \tag{5.24}
$$

Simplifying the Eq. (5.24), we obtain the following method for the differential Eq. (3.1) at the grid point $(x_{\bar{l}}, t_j)$, for $l=\bar{l}$:

$$
\begin{aligned}
M_3T_{l-1}+M_1T_l+M_2T_{l+1} &= A_3\beta^-T_{tl-1}+(A_1\beta^-+A_4\beta^+)T_{tl}+A_2\beta^+T_{tl+1}\\
&\quad + A_3\gamma^-T_{l-1}+(A_1\gamma^-+A_4\gamma^+)T_l+A_2\gamma^+T_{l+1}+F,
\end{aligned} \tag{5.25}
$$

where,

$$
\begin{aligned}
M_1 &= X_1 - X_3,\\
M_2 &= X_3 - X_2,\\
M_3 &= X_2 - X_1,
\end{aligned}
$$

and

$$
\begin{aligned}
A_1 &= (X_1-X_3)\frac{h_1^2}{3!\kappa^-}\left[1-\left(2+\frac{2h_1\kappa^{-'}}{\kappa^-}\right)\frac{h_3}{h}\right]+(X_2-X_1)\frac{h_3^2}{3!\kappa^-}\left(2+\frac{2h_3\kappa^{-'}}{\kappa^-}\right)\frac{h_3}{h},\\
A_2 &= (X_3-X_2)\frac{h_2^2}{3!\kappa^+}\left[\left(2-\frac{2h_2\kappa^{+'}}{\kappa^+}\right)\frac{\kappa^+h_1}{\kappa^+h_1+\kappa^-h_2}+1\right],\\
A_3 &= (X_2-X_1)\frac{h_3^2}{3!\kappa^-}\left[1-h_1/h\left(2+\frac{2h_3\kappa^{-'}}{\kappa^-}\right)\right]+(X_1-X_3)\frac{h_1^3}{3!\kappa^-h}\left(2+\frac{2h_1\kappa^{-'}}{\kappa^-}\right),\\
A_4 &= (X_3-X_2)\frac{h_2^2}{3!\kappa^+}\left[\left(2-\frac{2h_2\kappa^{+'}}{\kappa^+}\right)\frac{\kappa^-h_2}{\kappa^+h_1+\kappa^-h_2}\right],
\end{aligned}
$$

and F_l consists of the terms obtained for the forcing function.
Applying CN method in time direction from the Eq. (5.25), we obtain the following scheme, for $l = \bar{l}$

$$
\begin{aligned}
&\frac{1}{2}\left(M_3(T_{l-1}^{j+1}+T_{l-1}^{j})+M_1(T_{l}^{j+1}+T_{l}^{j})+M_2(T_{l+1}^{j+1}+T_{l+1}^{j})\right)\\
&=A_3\beta^{-}\frac{T_{l-1}^{j+1}-T_{l-1}^{j}}{\Delta t}+(A_1\beta^{-}+A_4\beta^{+})\frac{T_{l}^{j+1}-T_{l}^{j}}{\Delta t}+A_4\beta^{+}\frac{T_{l+1}^{j+1}-T_{l+1}^{j}}{\Delta t}\\
&+A_3\gamma^{-}\frac{T_{l-1}^{j+1}+T_{l-1}^{j}}{2}+(A_1\gamma^{-}+A_4\gamma^{+})\frac{T_{l}^{j+1}+T_{l}^{j}}{2}+A_4\gamma^{+}\frac{T_{l+1}^{j+1}+T_{l+1}^{j}}{2}\\
&+\frac{F_l^{j}+F_l^{j+1}}{2},
\end{aligned}
\tag{5.26}
$$

The Eq. (5.26) can further be re-written as,

$$
\begin{aligned}
&\left(\frac{M_3}{2}-\frac{A_3\beta^{-}}{\Delta t}-\frac{A_3\gamma^{-}}{2}\right)T_{l-1}^{j+1}+\left(\frac{M_1}{2}-\frac{A_1\beta^{-}+A_4\beta^{+}}{\Delta t}-\frac{A_1\gamma^{-}+A_4\gamma^{+}}{2}\right)T_{l}^{j+1}\\
&+\left(\frac{M_2}{2}-\frac{A_2\beta^{+}}{\Delta t}-\frac{A_2\gamma^{+}}{2}\right)T_{l+1}^{j+1}=\left(-\frac{A_3\beta^{-}}{\Delta t}-\frac{A_3\gamma^{-}}{2}-\frac{M_3}{2}\right)T_{l-1}^{j}\\
&+\left(-\frac{M_1}{2}-\frac{A_1\beta^{-}-A_4\beta^{+}}{\Delta t}-\frac{A_1\gamma^{-}+A_4\gamma^{+}}{2}\right)T_{l}^{j}+\left(-\frac{A_2\beta^{+}}{\Delta t}-\frac{A_2\gamma^{+}}{2}-\frac{M_2}{2}\right)T_{l+1}^{j}\\
&+\frac{F_l^{j}+F_l^{j+1}}{2},
\end{aligned}
\tag{5.27}
$$

for $l = \bar{l}$. Following the same approach as in Eq. (5.25), we can derive a scheme for $x_{\bar{l}}$, $x_{\bar{l}+1}$ and $x_{\bar{l}+2}$.

The method obtained by the Eqs. (3.8), (5.27) together with boundary conditions give rise to a tri-diagonal matrix structure, which can further be solved using Thomas algorithm.

6. Numerical results

In this section, first to show the efficacy of our method, we have considered some examples whose exact solution is known. We compare the numerical solution obtained with the exact solution and draw some conclusions from it. In the examples, one can observe that $T^{-} = T^{+}$ and $\kappa^{-}T_x^{-} = \kappa^{+}T_x^{+}$.

Example 6.1. Let us consider the differential Eq. (3.2), with the initial conditions given by

$$
T(x,0)=\begin{cases}(x-\alpha)^3, & 0\le x\le\alpha,\\ (x-\alpha)^4, & \alpha<x\le 1.\end{cases}
$$

and the boundary conditions: $T(0,t) = -\alpha^3 e^{-t}, t \ge 0$ and $T(1,t) = (1-\alpha)^4 e^{-t}, t \ge 0$, where $\alpha \in (0,1)$. The source function f is given by

$$
f(x,t)=\begin{cases}10(x-\alpha)^3e^{-t}+12(x-\alpha)e^{-t}-10(x-\alpha)^3e^{-t}, & 0\le x\le\alpha,\\ 15(x-\alpha)^4e^{-t}+144(x-\alpha)^2e^{-t}-2(x-\alpha)^4e^{-t}, & \alpha<x\le 1.\end{cases}
$$

In this example, we choose the coefficients κ, β and γ to be piece wise constants in the domain $[0,1]$ defined as follows

$$\kappa = \begin{cases} \kappa^- = 2, & 0 \le x \le \alpha, \\ \kappa^+ = 12, & \alpha < x \le 1, \end{cases}$$

$$\beta = \begin{cases} \beta^- = 10, & 0 \le x \le \alpha, \\ \beta^+ = 15, & \alpha < x \le 1, \end{cases}$$

$$\gamma = \begin{cases} \gamma^- = 10, & 0 \le x \le \alpha, \\ \gamma^+ = 2, & \alpha < x \le 1. \end{cases}$$

The exact solution to the above problem is given by

$$T(x,t) = \begin{cases} (x-\alpha)^3 e^{-t}, & 0 \le x \le \alpha, \\ (x-\alpha)^4 e^{-t}, & \alpha < x \le 1. \end{cases}$$

We solved the differential equation for two different cases. In the first case, we choose the value of $\alpha = 0.2$. Here, the interface falls at a grid point. The maximum absolute errors between the exact and numerical solutions obtained by the proposed method and the order of convergence are listed in the Table 1 for different grid sizes. Our method gives fourth-order accuracy for the choice $k \propto h^2$.

In case, when the interface does not fall at the grid point, let us choose $\alpha = 0.201$ and list the maximum absolute errors between the exact and numerical solutions and fourth order of convergence in the Table 2 for different grid sizes. Figure 2 represents the comparison between analytical solution and the numerical solution at final time $t = 1$, for

Table 1. Maximum absolute errors obtained for Example 6.1, when the interface falls at a grid point $\alpha = 0.2$.

h	$\frac{1}{10}$	$\frac{1}{20}$	$\frac{1}{40}$	$\frac{1}{80}$
k	$\frac{1}{40}$	$\frac{1}{160}$	$\frac{1}{640}$	$\frac{1}{2560}$
error	1.999e-01	1.120e-02	6.623e-04	1.863e-05
order	-	4.12	4.12	4.53

Table 2. Maximum absolute errors obtained for Example 6.1, when interface falls at a non-grid point $\alpha = 0.201$.

h	$\frac{1}{10}$	$\frac{1}{20}$	$\frac{1}{40}$	$\frac{1}{80}$
k	$\frac{1}{40}$	$\frac{1}{160}$	$\frac{1}{640}$	$\frac{1}{2560}$
error	1.830e-01	9.400e-03	3.850e-04	1.882e-05
order	-	4.28	4.61	4.35

interface lying at $\alpha = 0.5$. From the figure it can be observed that the numerical solution is in close agreement with the analytical solution throughout the domain. The agreement near the interface shows that our numerical method handles the discontinuity in the coefficients effectively. This confirms the accuracy and reliability of our numerical method.

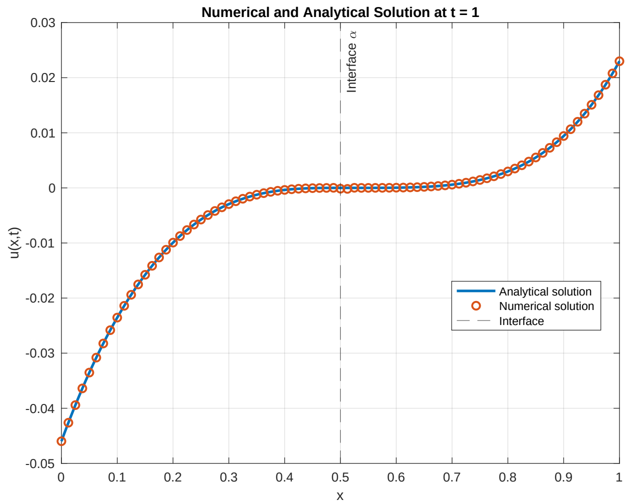

FIGURE 2. Numerical solution and analytic solution of Example 6.1 at final time $t = 1$ and interface $\alpha = 0.5$.

Example 6.2. Let us consider the differential Eq. (3.2). Here, we choose the coefficient κ to be a variable function of x,

$$\kappa = \begin{cases} \kappa^- = 1, & 0 \leq x \leq \alpha, \\ \kappa^+ = x + 10, & \alpha < x \leq 1. \end{cases}$$

with the initial conditions given by

$$T(x,0) = \begin{cases} (x-\alpha)^3, & 0 \leq x \leq \alpha, \\ (x-\alpha)^4, & \alpha < x \leq 1. \end{cases}$$

and the boundary conditions: $T(0,t) = -\alpha^3 e^{-t}, t \geq 0$ and $T(1,t) = (1-\alpha)^4 e^{-t}, t \geq 0$, for $\alpha \in (0,1)$. The source function f is given by

$$f(x,t) = \begin{cases} 20(x-\alpha)^3 e^{-t} + 6(x-\alpha)e^{-t} - (x-\alpha)^3 e^{-t}, & 0 \leq x \leq \alpha, \\ 10(x-\alpha)^4 e^{-t} + 12(x+10)(x-\alpha)^2 e^{-t} + 4(x-\alpha)^3 e^{-t}, & \alpha < x \leq 1. \end{cases}$$

we choose β and γ to be piece wise constants in the domain $[0,1]$ defined as follows

$$\beta = \begin{cases} \beta^- = 20, & 0 \leq x \leq \alpha, \\ \beta^+ = 10, & \alpha < x \leq 1. \end{cases}$$

$$\gamma = \begin{cases} \gamma^- = 1, & 0 \leq x \leq \alpha, \\ \gamma^+ = 0, & \alpha < x \leq 1. \end{cases}$$

The exact solution to the above problem is given by

$$T = \begin{cases} (x-\alpha)^3 e^{-t}, & 0 \leq x \leq \alpha, \\ (x-\alpha)^4 e^{-t}, & \alpha < x \leq 1. \end{cases}$$

In Table 3, we list the maximum absolute errors and order of convergence for $\alpha = 0.5$ for different grid sizes. When the interface lies at a non-grid point $\alpha = 0.501$, the maximum absolute errors and the order of convergence are tabulated in Table 4. From both the tables, it can be seen that the order of convergence is four.

TABLE 3. maximum absolute errors and orders obtained for Example 6.2, when interface falls at grid point $\alpha = 0.5$.

h	$\frac{1}{10}$	$\frac{1}{20}$	$\frac{1}{40}$	$\frac{1}{80}$
k	$\frac{1}{40}$	$\frac{1}{160}$	$\frac{1}{640}$	$\frac{1}{2560}$
error	3.100e-02	1.500e-03	9.962e-05	5.812e-06
order	-	4.37	3.91	4.10

TABLE 4. Maximum absolute errors and orders obtained for Example 6.2, when interface falls at non-grid $\alpha = 0.501$.

h	$\frac{1}{10}$	$\frac{1}{20}$	$\frac{1}{40}$	$\frac{1}{80}$
k	$\frac{1}{40}$	$\frac{1}{160}$	$\frac{1}{640}$	$\frac{1}{2560}$
error	2.800e-02	1.000e-3	6.322e-05	2.440e-06
order	-	4.52	4.25	4.69

Example 6.3. Let us consider the differential equation [1], given by

$$\frac{\partial T}{\partial t} = \nabla \cdot (\kappa \nabla T) + f,$$

with the initial conditions

$$T(x,0) = \begin{cases} x^8, & 0 \le x \le \alpha, \\ \dfrac{1}{2}\left(\dfrac{1}{256} + x^8\right), & \alpha < x \le 1. \end{cases}$$

and the boundary conditions: $T(0,t) = 0, t \ge 0$ and $T(1,t) = \frac{257}{512}e^{-t}, t \ge 0$.
The source function f is given by

$$f(x,t) = \begin{cases} \left(x^8 + 56x^6\right) e^{-t}, & 0 \le x \le \alpha, \\ \left(\dfrac{1}{512} + \dfrac{x^8}{2} + 56x^6\right) e^{-t}, & \alpha < x \le 1. \end{cases}$$

The value of κ in the domain $[0,1]$ is defined as

$$\kappa = \begin{cases} \kappa^- = 1, & 0 \le x \le \alpha, \\ \kappa^+ = 2, & \alpha < x \le 1. \end{cases}$$

The exact solution to this problem is given by

$$T(x,t) = \begin{cases} x^8 e^{-t}, & 0 \le x \le \alpha, \\ \dfrac{1}{2}\left(\dfrac{1}{256} + x^8\right) e^{-t}, & \alpha < x \le 1. \end{cases}$$

We choose the location of the interface $\alpha = 0.5$. We compared the maximum absolute errors and convergence rates obtained by the proposed method with those of the second order Difference Potentials Method (DPM2) [1], and the Immersed Interface Method [8]. From the Table 5, it can easily be observed that the present method gives fourth order of convergence even for coarser time step k.

Table 5. Comparisons of maximum absolute errors and orders for Example 6.3, when $\alpha = 0.5$.

N	Present method	order	DPM2 error	order	IIM error	order
20	$2.642e-06$	–	$3.208e-03$	–	$3.307e-03$	–
40	$2.004e-07$	3.721	$8.580e-04$	1.902	$8.275e-04$	1.998
80	$1.692e-08$	3.566	$2.089e-04$	2.038	$2.069e-04$	1.999
160	$9.217e-10$	4.198	$5.127e-05$	2.026	$5.173e-05$	1.999

7. Applications

This paper provides a high-order numerical solution to the Pennes bioheat conduction equation. Two tissues have different thermophysical properties. As the tumors are sites of intense heat activity so the metabolic heat production and blood perfusion rate will differ from the normal tissue.

The disparity between these values has a significant impact on the hyperthermia treatment. Various parameters affect the treatment of the cancerous cell like thermal conductivity κ, blood and tissue density ρ, ρ_b, and specific heat of blood and tissue C, C_b.The effective thermal diffusivity of the tumour tissue will be slightly higher than that of the healthy tissue. Let the thickness of the cancerous tissue be 1cm and the thickness of healthy tissue be 2.5cm. The continuity of temperature is maintained and the continuity of the heat flux, so $T^-{=}T^+$ and $\kappa^- T_x^-{=}\kappa^+ T_x^+$.

As the human thermo-regulatory system has the tendency to maintain a regular temperature of 37^oC, the initial temperature T_0 will be taken as 37^oC and the temperature of blood $T_b = 37^oC$. We take the following data for healthy tissue and the cancerous tissue respectively [2],

$\{\rho^-, \rho^+\} = \{1.1, 1.0\}\, g/cm^3$, $\{C^-, C^+\} = \{4.2, 4.2\}\, J/(gC)$, and $\{\kappa^-, \kappa^+\} = \{5.5 \times 10^{-3}, 5.0 \times 10^{-3}\}\, W/(cmC)$. We consider $C_b = 4.2\, J/(gC)$ and $\{\omega_b^-, \omega_b^+\} = \{10^{-3}, 10^{-3}\}\, g/(cm^3 s)$.

Firstly, we choose heat generation P as the quadratic polynomial in terms of the spacial variation given by

$$P = P_0 + P_1 x + P_2 x^2,$$

where P_0, P_1 and P_2 are constants, which takes the following values in our problem,

$$P_0 = 0.1W/cm^3, P_1 = 0.01W/cm^4, P_2 = -0.05W/cm^5.$$

The model given by the Eq. (2.2) is solved numerically and Figure 3 is drawn to show the temperature distribution with along the distance x at different time levels $t = 10s, 20s, 30s$ and $40s$. It can be seen from the figure that the temperature increases with time.

Now, solving numerically by taking P as constant, $P = 1.5Wcm^3$ and Figure 4 is drawn to see the variation in temperature with respect to distance at different times $t = 5s$, $10s$, $15s$, $20s$, $25s$, $30s$. From Figures 3 and 4, we can see that the temperature in the cancerous tissue, is increasing as the time duration of heating is increased. This can be observed physically, as longer exposure to external heat allows the tissue to absorb more energy.

Figure 5 shows the variation in temperature for different values of external heat P at time $t = 20s$. Here we have chosen different constant values of P as $1.5W/cm^3$, $1.6W/cm^3$, $1.7W/cm^3$, $1.8W/cm^3$, $1.9W/cm^3$, $2.0W/cm^3$, $2.1W/cm^3$, $2.2W/cm^3$ and $2.3W/cm^3$. This shows that the temperature field is strongly influenced by the magnitude of the heat source. From Figure 5, we can observe the increase in temperature on increasing the power. The temperature profile at two spatial positions $x = 1.25cm$ and $x = 1.5cm$ at the time $t = 40s$ is shown in Figure 6. In the paper [6], Klinger has explained how the rate of decrease of the temperature is correlated with the blood perfusion. Figure 7 shows the effect on temperature pattern without perfusion and with perfusion taken as $8 \times 10^{-3} g/(cm^3 s)$. Here, we choose $P = 1.2W/cm^3$ and time $40s$. From Figure 7, we can see that the perfusion decreases the temperature due to its ability to balance the relative temperature of the local area. As blood circulation act as sink and carries away the excess energy from the affected region.

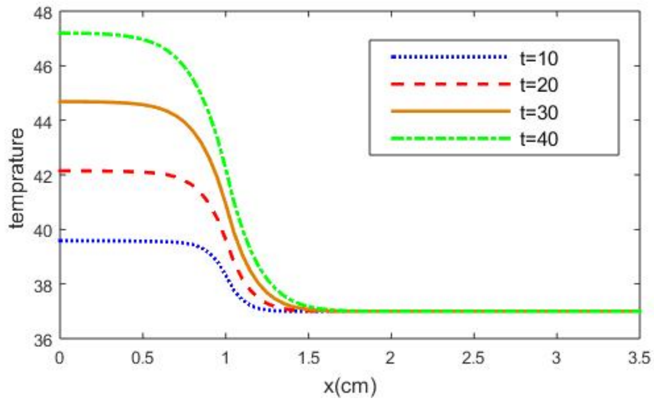

FIGURE 3. Temperature distribution at different time levels when the heat generation is $P = P_0 + P_1 x + P_2 x^2$.

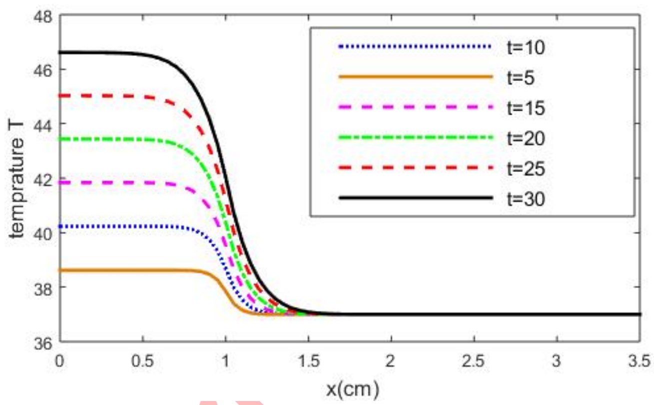

FIGURE 4. Temperature distribution at different times in case when heat generation is constant $P = 1.5 W cm^3$.

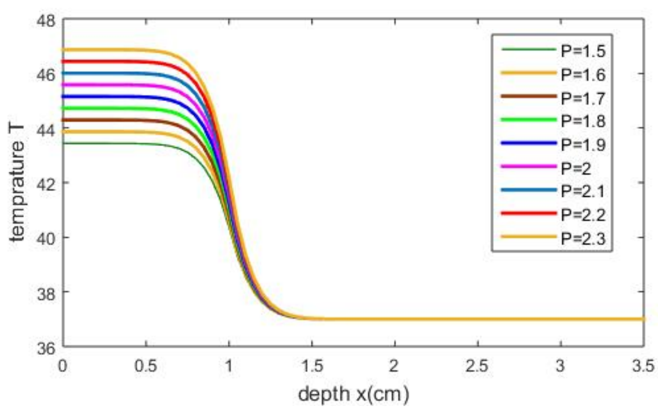

FIGURE 5. effect of heat generation due to external heat to the temperature dispense.

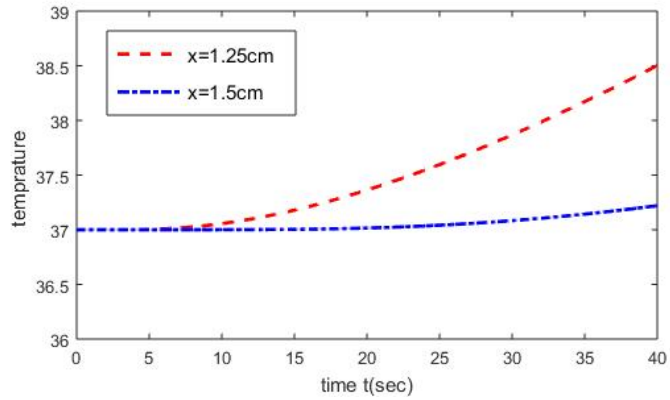

FIGURE 6. temperature profile at two different positions at time=40 seconds.

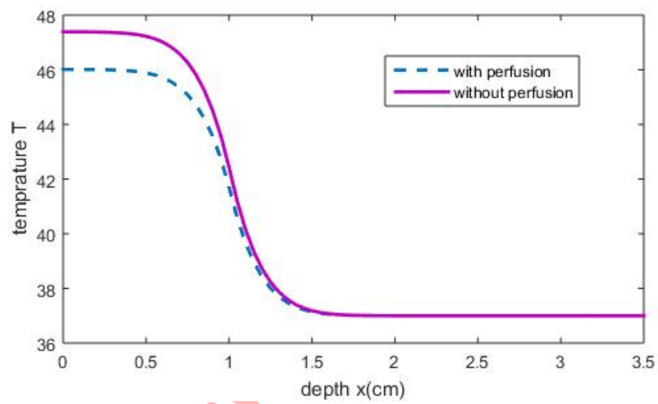

FIGURE 7. comparison in temperature profile with and without perfusion

8. Conclusion

In hyperthermia therapy body tissue is heated to kill cancer cells. Extreme heat supplied during the hyperthermia treatment may damage the healthy tissue surrounding the cancerous tissue. In this paper, the behavior of temperature in living tissues is studied during hyperthermia treatment using Penne's bioheat transfer equation. A high-order compact finite difference numerical method has been developed for the differential equation with piece-wise continuous coefficients. Some test problems for which the analytical solution are known have been solved to demonstrate the accuracy and order of convergence of the method. The behavior of temperature with constant and variable heat generation due to an external heat source is examined. The effect of blood perfusion on temperature patterns is also studied. Although we cannot control the damage to the healthy tissue completely, we can minimize it to a great extent by choosing the right amount of heat.

Declarations

- Conflict of interest/Competing interests
  The authors declare that they have no conflict of interest.
- Availability of data and materials
  The authors declare that no data was used for the research described in this article.

Acknowledgment

The authors would like to thank the anonymous reviewers whose suggestions have improved the quality of the paper. The third author would like to thank the funding agency University Grants Commission, India for providing the fellowship for this research.

References

[1] J. Albright, Y. Epshteyn, and K. R. Steffen, *High-order accurate difference potentials methods for parabolic problems*, Applied Numerical Mathematics, *93* (2015), 87–106.

[2] H. G. Bagaria and D. T. Johnson, *Transient solution to the bioheat equation and optimization for magnetic fluid hyperthermia treatment*, International Journal of Hyperthermia, *21* (2005), 57–75.

[3] Z.-S. Deng and J. Liu, *Analytical study on bioheat transfer problems with spatial or transient heating on skin surface or inside biological bodies*, Journal of Biomechanical Engineering, *124* (2002), 638–649.

[4] M. A. Giordano, G. Gutierrez, and C. Rinaldi, *Fundamental solutions to the bioheat equation and their application to magnetic fluid hyperthermia*, International Journal of Hyperthermia, *26* (2010), 475–484.

[5] K. Jeziorski, *Hyperthermia in rheumatic diseases. A promising approach?*, Reumatologia/Rheumatology, *56* (2018), 316–320.

[6] H. G. Klinger, *Heat transfer in perfused biological tissue-I: General theory*, Bulletin of Mathematical Biology, *36* (1974), 403–415.

[7] R. J. LeVeque and Z. Li, *The immersed interface method for elliptic equations with discontinuous coefficients and singular sources*, SIAM Journal on Numerical Analysis, *31* (1994), 1019–1044.

[8] Z. Li and K. Ito, *The Immersed Interface Method: Numerical Solutions of PDEs Involving Interfaces and Irregular Domains*, Frontiers in Applied Mathematics, Vol. 33, Society for Industrial and Applied Mathematics, Philadelphia, PA, 2006.

[9] K. C. Liu and H. T. Chen, *Analysis for the dual-phase-lag bio-heat transfer during magnetic hyperthermia treatment*, International Journal of Heat and Mass Transfer, *52* (2009), 1185–1192.

[10] K. C. Liu and P. J. Cheng, *Finite propagation of heat transfer in a multilayer tissue*, Journal of Thermophysics and Heat Transfer, *22* (2008), 775–782.

[11] R. K. Mohanty, M. K. Jain, and D. Kumar, *Single cell finite difference approximations of* $O(kh^2 + h^4)$ *for* $\partial u/\partial x$ *for one space dimensional nonlinear parabolic equation*, Numerical Methods for Partial Differential Equations, *16* (2000), 408–415.

[12] H. H. Pennes, *Analysis of tissue and arterial blood temperatures in the resting human forearm*, Journal of Applied Physiology, *1* (1948), 93–122.

[13] A. V. Presgrave, R. O. C. Guedes, and F. Scofano Neto, *Analysis of skin burn injuries through integral transform techniques*, in Proceedings of the 11th Brazilian Congress of Thermal Sciences and Engineering, ABCM, Curitiba, PR, Brazil, 2006, 5–8.

[14] T. C. Shih, P. Yuan, W. L. Lin, and H. S. Kou, *Analytical analysis of the Pennes bioheat transfer equation with sinusoidal heat flux condition on skin surface*, Medical Engineering and Physics, *29* (2007), 946–953.

[15] S. Singh, S. Singh, and Z. Li, *A high order compact scheme for a thermal wave model of bio-heat transfer with an interface*, Numerical Mathematics: Theory, Methods and Applications, *11* (2018), 321–337.

[16] D. A. Torvi and J. D. Dale, *A finite element model of skin subjected to a flash fire*, Journal of Biomechanical Engineering, *116* (1994), 250–255.

[17] S. Toraya Brown and S. Fiering, *Local tumour hyperthermia as immunotherapy for metastatic cancer*, International Journal of Hyperthermia, *30* (2014), 531–539.

[18] M. Tunç, U. Çamdali, C. Parmaksizoğlu, and S. Çikrikçi, *The bio-heat transfer equation and its applications in hyperthermia treatments*, Engineering Computations, *23* (2006), 451–463.